The Design of Extended Bandwidth Shape Memory Alloy Actuators

JASON B. DITMAN
GM Powertrain Division, General Motors Corporation, Ypsilanti, Michigan

LAWRENCE A. BERGMAN* AND TSU-CHIN TSAO
University of Illinois at Urbana-Champaign, 104 South Wright Street, Urbana, Illinois 61801

ABSTRACT: Extending the usable bandwidth of shape memory alloy actuators for vibration control is investigated, both analytically and experimentally. The differential actuator, which uses SMA wires in agonist-antagonist pairs, is a potential solution. Simulation shows that only modest power requirements are necessary to achieve bandwidths between 10 and 20 Hz.

INTRODUCTION

As space structures become more lightweight and flexible, control of system responses due to both external and internal forces is increasingly important. A small maneuver by a space structure with flexible appendages induces low frequency vibration which requires many cycles to attenuate by passive means. Traditionally, such response has been attenuated by applying passive control systems such as tuned mass dampers and viscoelastic damping materials. These can be effective but, in extreme cases, may provide insufficient improvement in performance. For example, an antenna on a communications satellite may be required to slew rapidly, stop, and send or receive information in a fraction of a second. Such performance objectives are inconsistent with the capabilities of passive vibration control systems and lead the designer to active strategies.

Recently, a large body of research has been devoted to developing applications for the unique properties of shape memory alloys (see, for example, Buehler and Wiley, 1965; Cross, et al., 1970; Jackson et al., 1972; Wayman and Duerig, 1990). Shape memory materials possess the ability to remember their initial configuration. After deformation, these materials return to their initial shape when heated through a transformation region. In addition, the material properties of shape memory alloys change throughout the phase transformation. It is these unique characteristics that make shape memory alloys potentially valuable components in smart material systems.

In terms of application to structural control, Rogers and coworkers (Liang et al., 1990, 1991, 1992; Rogers et al., 1988, 1989a, 1989b, 1990a, 1990b, 1991, 1993) have made significant contributions, both analytically and experimentally. Rogers, Liang, and Jia (1989a) and Rogers and Barker (1990a) have used active strain energy tuning (ASET) and active properties tuning (APT) to alter the vibrational characteristics of composite plates containing embedded shape memory alloy wires. In both cases, increasing the effective stiffness of the structure caused an upward shift in the natural frequencies of vibration. Selective activation of the embedded wires was also shown to be useful in altering mode shapes. Baz and Ro (1992) developed a thermal finite element model of shape memory alloy reinforced composite beams and investigated the effect of selective activation on response. In other applications, Chaudhry and Rogers (1991a, 1991b) used the forces developed during restrained recovery to control buckling of cantilevered beams. Wires embedded along the neutral axis of a beam generate recovery forces that oppose buckling. The inplane tensile loads add to the overall structural stiffness, thereby increasing the critical buckling load.

The above systems can be considered to be passive in nature because they do not require that the shape memory alloy wires be thermally cycled. The use of shape memory materials as active components in vibration control systems has been studied by Baz and coworkers (1990a, 1990b) and Rogers and coworkers (1988, 1989a, 1989b, 1990a, 1991, 1993). Baz, Imam, and McCoy (1990a) used the shape recovery effect to actively control the vibration of a cantilevered beam. Wires mounted to the surface of the beam were used to generate control forces opposing low frequency vibration. The bandwidth of such a control system, however, is limited by the ability to cool the nitinol wires for the next cycle. Wilson, Anderson, Rempt, and Ikegami (1990) extended the bandwidth of such a system by using multiple shape memory alloy wires attached to the surface of a cantilevered beam. The multiple wire configuration allowed a higher actuation frequency to be achieved by heating a wire every other cycle rather than on every cycle. This provided more cooling time for each wire. Liang and

*Author to whom correspondence should be addressed.

1045-389X/96/06 0635-11 $10.00/0

Rogers (1990) extended the capabilities of SMA-based actuator systems by developing design criteria for actuators employing shape memory alloy wires. The performance of these actuators is highly dependent on the material properties of the shape memory alloy wires and the means by which the wires are cooled. Baz, Imam, and McCoy (1990a, 1990b) showed experimentally that the maximum attainable bandwidth of SMA-based actuators is highly dependent on the means of cooling the wires. In both cases, only relatively low bandwidths were achieved. The objective of the work reported herein is to demonstrate a concept by which the usable bandwidth of SMA-based actuators can be extended.

THE DIFFERENTIAL FORCE ACTUATOR

Configuration

A diagram of the differential force actuator is shown in Figure 1 (Quatrone, 1992). The actuator consists of two groups (A and B), each with N shape memory alloy wires. The groups form an agonist-antagonist pair with one group providing the deformation force and the other providing the restoring force. The group A wires are of length L_A and diameter d_A, while the group B wires are of length L_B and diameter d_B. In order to simplify the notation, both groups of wires are assumed to have the same material properties and transformation temperatures (see for example, Materials Electronics Products Corp., 1990).

The temperature of each group of wires is to be controlled independently. As a result, the chambers housing the two groups will be thermally insulated from each other. Two thermocouples, one for each group, will be used to provide temperature feedback. All of the wires in a group are connected in series to allow for resistive heating, and thermoelectric devices will be used to maintain predetermined ambient temperatures. A set of thermoelectric devices will be used for each chamber to allow different ambient temperatures to be maintained.

The typical operation of this actuator system is illustrated in Figure 2. First, wire group B is heated while the temperature of group A is held constant. The group B wires are prestrained, and heating causes the deformed martensite to revert to austenite. The transformation process recovers the prestrain and produces a force against the group A wires. The group A wires serve as a nonlinear spring with a high initial stiffness and a lower stiffness during the transformation. If the maximum force produced by the group B wires cannot get the group A wires past the first yield strength, the group A wires will be deforming within the linear elastic range. In this case, the wires in group A function as a bias spring (Liang and Rogers, 1991). The advantage of using shape memory alloy wires over a coil spring to provide the restoring force becomes evident when the stress in the wires surpasses the yield stress. Once the stress in the group A wires is above the first yield strength, the wires undergo a stress induced martensitic transformation. This process stores energy that will later be used to restore the actuator

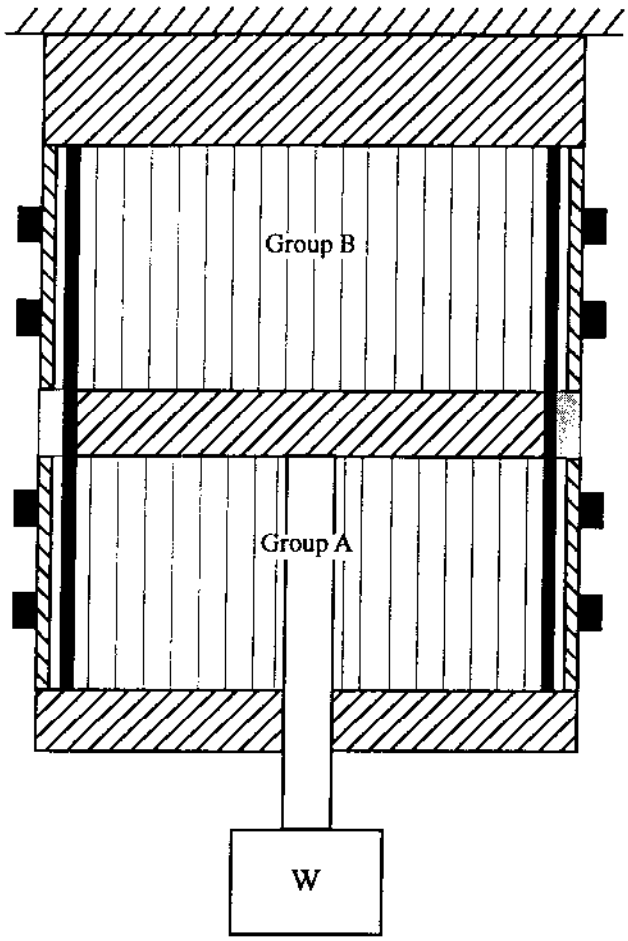

Figure 1. Differential force actuator configuration.

to its initial position. During the restoration process, the group A wires are heated while the group B wires cool. The group A wires generate a much greater recovery force, due to the energy stored in the martensitic structures, that pulls the group B wires back to the initial position. The external stress on the group B wires will increase the martensitic transformation temperature, resulting in an earlier martensitic transformation and shorter cycle times. The actuator can be heated for the next cycle once the group wires have returned to the initial state.

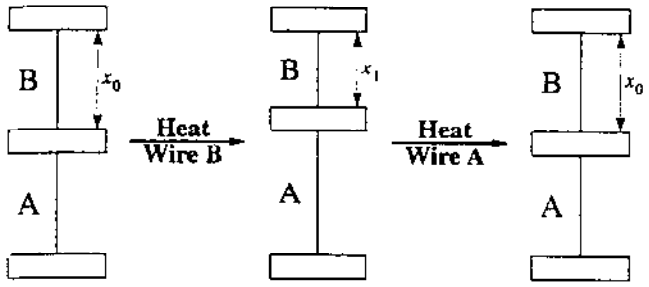

Figure 2. Operating cycle of the differential force actuator.

Differential Force Relation

The rate form of the constitutive relations for wire groups A and B can be expressed as (Liang and Rogers, 1991; Tanaka et al., 1992):

$$\left.\begin{aligned}\dot{\sigma}^{A_i} &= D\dot{\epsilon}^{A_i} + \Omega\dot{\xi}^{A_i} + \theta\dot{T}^{A_i}\\ \dot{\sigma}^{B_i} &= D\dot{\epsilon}^{B_i} + \Omega\dot{\xi}^{A_i} + \theta\dot{T}^{B_i}\end{aligned}\right\} \quad i = 1,2,\ldots,N \tag{1}$$

where N is the total number of wires in each of groups A and B. The subscript, i, is used to refer to the properties of an individual wire, and the overdot indicates differentiation with respect to time. The equilibrium condition of the system is given by

$$\Sigma\sigma^{A_i} = \Sigma(\sigma^{B_i} - \sigma_0^{B_i}) \tag{2}$$

It is assumed that the total force exerted by each group is evenly distributed among all of the wires, which results in the relations

$$\begin{aligned}\sigma^{A_1} &= \sigma^{A_2} = \cdots = \sigma^{A_{n_A}} = \sigma^A\\ \sigma^{B_1} &= \sigma^{B_2} = \cdots = \sigma^{B_{n_B}} = \sigma^B\end{aligned} \tag{3}$$

where n_A and n_B refer to the number of active wires in each group. Substituting (3) into (2) yields the generalized equilibrium equation,

$$n_A\sigma^A = n_B(\sigma^B - \sigma_0^B) \tag{4}$$

The effect of activating only a small number of the wires in a group will be discussed in a later section.

The geometric compatibility between groups A and B requires that

$$-\Delta x_A = \Delta x_B \tag{5}$$

Using the strain-displacement relationship $\Delta x = L(\epsilon - \epsilon_0)$, Equation (5) can be written as

$$-L_A(\epsilon^A - \epsilon_0^A) = L_B(\epsilon^B - \epsilon_0^B) \tag{6}$$

Differentiating Equation (6) yields the compatibility relation (Liang and Rogers, 1992)

$$-L_A\dot{\epsilon}^A = L_B\dot{\epsilon}^B \tag{7}$$

The rate form of the constitutive law for the actuator can be expressed as (Liang and Rogers, 1990, 1991)

$$L_A\dot{\sigma}^A - L_A\Omega\dot{\xi}^A - L_A\theta\dot{T}^A = -L_B\dot{\sigma}^B + L_B\Omega\dot{\xi}^B + L_B\theta\dot{T}^B \tag{8}$$

Note that, while subscripts i have been omitted for simplification, Equation (8) is the rate form of the constitutive law for a single wire pair. Moving the terms involving the group B wire to the left side and factoring out the wire lengths gives

$$L_A(\dot{\sigma}^A - \Omega\dot{\xi}^A - \theta\dot{T}^A) + L_B(\dot{\sigma}^B - \Omega\dot{\xi}^B - \theta\dot{T}^B) = 0 \tag{9}$$

Liang and Rogers (1991) showed that this equation could be integrated, resulting in

$$L_A(\sigma^A - \Omega\xi^A - \theta T^A) + L_B(\sigma^B - \Omega\xi^B - \theta T^B) = C_1 \tag{10}$$

where the constant C_1 depends on the initial conditions of the actuator. At this point, it will be assumed with no loss of generality that $L_A = L_B = L$ and $d_A = d_B = d$. Substituting the equilibrium Equation (4) into Equation (10) gives

$$\frac{n_A}{n_B}(\sigma^B - \sigma_0^B) - \Omega\xi^A - \theta T^A + \sigma^B - \Omega\xi^B - \theta T^B = C_1 \tag{11}$$

which is the generalized differential actuator relation. To solve for the unknown constant, let $\sigma^B = \sigma_0^B$ and substitute into Equation (11) to obtain

$$C_1 = -\Omega\xi_0^A - \theta T_0^A + \sigma_0^B - \Omega\xi_0^B - \theta T_0^B \tag{12}$$

Substituting Equation (12) into Equation (11) and solving for σ^B yields the generalized stress-temperature relation for the differential actuator

$$\sigma^B = \sigma_0^B - \frac{\begin{matrix}[\Omega(\xi^A - \xi_0^A) + \theta(T^A - T_0^A)\\ + \Omega(\xi^B - \xi_0^B) + \theta(T^B - T_0^B)]\end{matrix}}{1 + n_B/n_A} \tag{13}$$

Defining the quantities θ'' and Ω'' such that

$$\theta'' = \frac{\theta}{1 + n_B/n_A} \tag{14}$$

$$\Omega'' = \frac{\Omega}{1 + n_B/n_A} \tag{15}$$

the generalized stress-temperature relation becomes

$$\sigma^B = \sigma_0^B - \Omega''(\xi^A - \xi_0^A) - \theta''(T^A - T_0^A) - \Omega''(\xi^B - \xi_0^B) - \theta''(T^B - T_0^B) \quad (16)$$

The actuator displacement is directly proportional to the strain in the group A wires and can be expressed as

$$x = L\epsilon^A \quad (17)$$

Equation (1) can be integrated with respect to time (Liang and Rogers, 1990) giving

$$\sigma_A - \sigma_0^A = D(\epsilon^A - \epsilon_0^A) + \Omega(\xi^A - \xi_0^A) + \theta(T^A - T_0^A) \quad (18)$$

$$\sigma_B - \sigma_0^B = D(\epsilon^B - \epsilon_0^B) + \Omega(\xi^B - \xi_0^B) + \theta(T^B - T_0^B)$$

Using Equation (4) to relate the stress in the two wire groups, the thermomechanical relations for the two groups can be equated resulting in

$$D(\epsilon^B - \epsilon_0^B) + \Omega(\xi^B - \xi_0^B) + \theta(T^B - T_0^B) = \frac{n_A}{n_B} \times [D(\epsilon^A - \epsilon_0^A) + \theta(T^A - T_0^A) + \Omega(\xi^A - \xi_0^A)] \quad (19)$$

Using Equation (7), the strain in the group A wires can then be expressed as

$$\epsilon^A = \frac{\Omega(\xi^B - \xi_0^B) + \theta(T^B - T_0^B) - \frac{n_A}{n_B}[\Omega(\xi^A - \xi_0^A) + \theta(T^A - T_0^A)]}{D(1 + n_B/n_A)} \quad (20)$$

Transient Response of SMA Wires

The transient thermal analysis of the wire is carried out using a lumped capacitance model. On heating from an initial temperature, T_0, and assuming convective boundary conditions, the temperature response can be expressed as

$$T - T_0 = T_f(1 - e^{-t/\tau}) \quad (21)$$

For resistive heating, the final stable temperature, T_f, and thermal time constant, τ, are given by

$$T_f = \frac{I^2R}{\pi dh}, \quad \tau = \frac{d\varrho c}{4h} \quad (22)$$

where I is the input current, R is the electrical resistance of the SMA wire, h is the heat transfer coefficient, ϱ is the density, and c is the specific heat. On cooling, the response can be expressed as

$$T - T_0 = (T_i - T_0)e^{-t/\tau} \quad (23)$$

where T_i is the temperature at the beginning of cooling cycle.

For the case of laminar flow around a rod of diameter d and subjected to a temperature gradient ΔT, the heat transfer coefficient can be approximated by (Holman, 1981)

$$h = 1.3\left(\frac{\Delta T}{d}\right)^{0.25} \quad (24)$$

Substituting Equation (24) into Equation (22) yields

$$T_f = \frac{I^2R}{1.3\pi d}\left(\frac{d}{\Delta T}\right)^{1/4}, \quad \tau = \frac{\varrho c}{4(1.32)}\left(\frac{d^{5/4}}{\Delta T^{1/4}}\right) \quad (25)$$

Temperature Control

Assume now that each of the groups is divided into subgroups containing n wires. The wires in the individual subgroups are connected in series and contain a thermocouple for temperature feedback. In this configuration, subgroups from chambers A and B form N/n agonist-antagonist pairs. The governing relations for each subgroup pair are the same as those given in the previous section but with $n_A = n_B = n$. The subgroup configuration has two benefits. First, it reduces the actuator reset problems encountered with previous actuator designs (Baz et al., 1990b; Liang and Rogers, 1992) by requiring that each subgroup be used only once out of every N/n cycles. Once one subgroup pair has completed its cycle, another pair will activate for the next. This eases the ambient temperature requirements, because each pair will now have N/n times longer to cool. If the actuator contained only one large group in each chamber, it would have to be kept to extremely low temperatures in order to achieve reasonable actuation frequencies. With the subgroup configuration, the actuator can complete a cycle by using one subgroup combination and begin another cycle with a different combination.

Since multiple subgroups are to be used, the ambient temperatures in two chambers only need to be low enough to ensure that the wires will reset before their next activation cycle. The temperature to which the wire must be cooled in order to achieve reset will be called T_{reset} which can be calculated from the thermomechanical relations. Thermoelectric devices will be used to maintain this temperature in the chambers. The only requirement on the actuator is that it contain sufficient subgroups to allow reset to occur before the next activation cycle.

A thermocouple will be used to monitor the temperature of each subgroup. During the heating portion of each subgroup's cycle, the thermocouple will activate an electrical switch. Once the wires in the subgroup reach the austenite finish temperature, the input signal is turned off, and the input for the other subgroup in the pair is turned on. This control scheme allows for high input voltages, which result in shorter cycle times.

The maximum temperature will also be used to control

the restoration process. Since the stress in wire group A is less than the stress in group B, the austenitic transformation temperatures of wire group A do not change as much as the martensitic transformation temperatures of group B. As a result, the transformation in the group A wires starts before the group B wires. Similarly, if the maximum temperature is high enough, the group A wires can be heated through their transformation before the group B wires begin the reverse transformation. This simplifies the analysis significantly.

DESIGN CASE STUDIES

In this section, the governing relations derived above will be used to simulate the response of the differential actuator. Liang and Rogers (1992) investigated single wire pair actuators and showed that they could be cycled more quickly than bias spring actuators. The case studies that follow will investigate the effect of the actuator physical parameters on actuation time, wire stress and actuator stroke. The parameters under investigation are the maximum wire temperature, the initial martensitic fractions of subgroups A and B, and the wire diameter. The results of these studies will be used to determine the effectiveness of this actuator at extended bandwidths. The case studies are carried out with reference to a baseline actuator system whose parameters are shown in Table 1.

Maximum Wire Temperature

Figure 3 shows the effect of the maximum attainable temperature on the heating cycle time for groups A and B. This figure indicates that, for equal maximum temperatures, the group B heating cycle is shorter than the group A cycle. The difference is due to the fact that the stress in the group A wires at the start of the restoration process is higher than the stress in the group B wires at the start of the deformation process. Higher stress results in higher austenitic transformation temperatures for the group A wires which causes longer actuation times. In order to maintain equal cycle times, the maximum attainable temperatures must be different. Using the governing relations, it is possible to predict what the two maximum temperatures need to be in order to maintain equal cycle times.

Table 1. Parameters for the baseline differential actuator.

Parameter	Value
M_s	−27°C
M_f	−34°C
A_s	−25°C
A_f	−14°C
D	7000 MPa
L	2 in
θ	0.1 MPa/°C
Ω	−70 MPa
T_f	100°C
T_0^A	−25°C
T_0^B	−25°C
d	0.025 in
ξ_0^A	0
ξ_0^B	0.6
$n = N$	1
W	1 lb

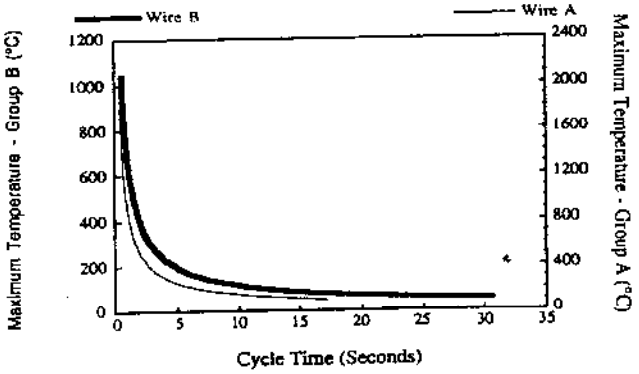

Figure 3. *Effect of the maximum wire temperature on the group A and B cycle times.*

Figure 3 also indicates the existence of a hyperbolic relationship between the maximum temperature and the heating cycle time. The figure shows that small increases in the maximum temperature can result in large decreases in the heating cycle time. For the group B wires, a change in the maximum temperature from 100°C to 200°C results in nearly a factor of three decrease in the heating cycle time. For the group A wires, a change in the maximum temperature from 200°C to 400°C results in a similar decrease.

Wire Diameter

The wire diameter has a significant effect on the thermal time constant. Figure 4 shows the effect of the wire diameter on the cycle time of wire groups A and B. Once again the difference in the cycle times for the two groups is due to the stress at the start of the respective transformations. The figure indicates that extremely small wire diameters can

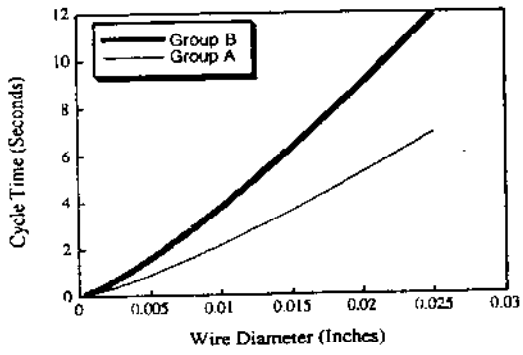

Figure 4. *Effect of wire diameter on the group A and B cycle times.*

result in a small heating cycle time for both groups. As a result, an actuator with a large number of small diameter wires can achieve higher actuation frequencies than one with a small number of large diameter wires.

Initial Martensitic Fraction of Wire B

The initial martensitic fraction of the group B wires has a significant effect on the response of the actuator as it determines the maximum actuator stroke. Figure 5 shows the effect of the initial martensitic fraction of the group B wires on the actuator stroke. The larger the martensitic fraction of the group B wires, the larger the maximum actuator stroke. Though an increased martensitic fraction increases the stroke, it also decreases the ability of the group A wires to return the actuator to the initial position. Figure 6 shows the reset gap versus the initial martensitic fraction of the group B wires. The reset gap is the difference between the initial actuator position and the position at the end of the group A transformation. The figure indicates that, if the group A wires have no initial martensitic fraction, they can only recover approximately half the deformation caused by the group B wires. As a result, in order to minimize the reset gap, the group A wires must also have an initial non-zero martensitic fraction. Figure 7 shows the martensitic fraction of the group A wires versus the reset gap. The figure shows that a martensitic fraction of 0.55 or above is required to achieve a complete cycle. From this result, a critical ratio between the two martensitic fractions can be derived. *Simulations indicate the ratio of the initial martensitic fraction of the group A wires to the initial martensitic fraction of the group B wires must be 0.9 or larger in order to achieve complete reset.*

Initial Martensitic Fraction of Wire A

The initial martensitic fraction of the group A wires has a larger effect on the cycle time than the group B wires. Figure 8 shows the cycle time plotted against the initial martensitic fraction of the group A wires. The cycle times increase because higher martensitic fractions result in

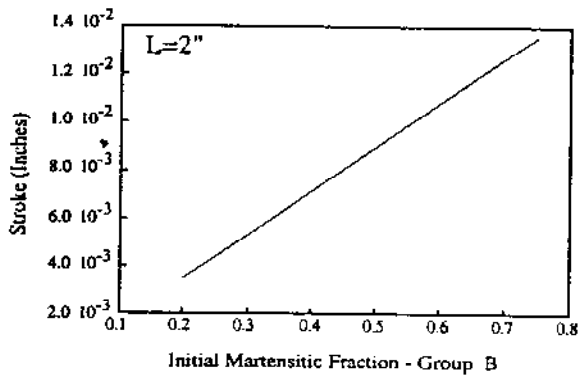

Figure 5. *Effect of the initial martensitic fraction of the group B wires on the actuator stroke.*

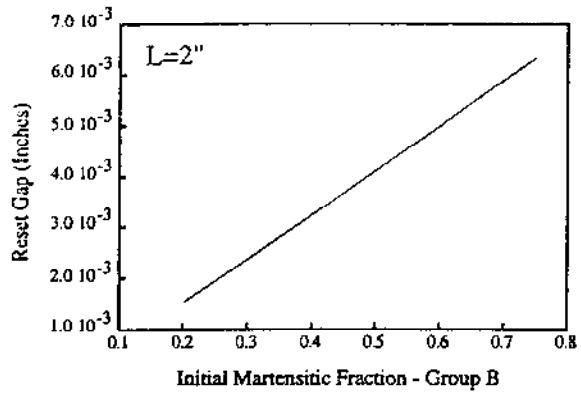

Figure 6. *Effect of the initial martensitic fraction of the group B wires on the actuator reset gap.*

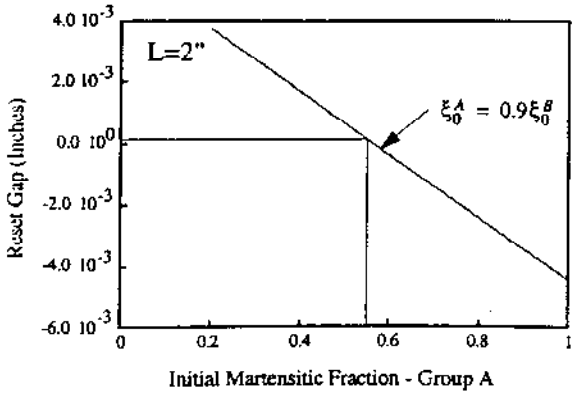

Figure 7. *Effect of the initial martensitic fraction of the group A wires on the actuator reset gap.*

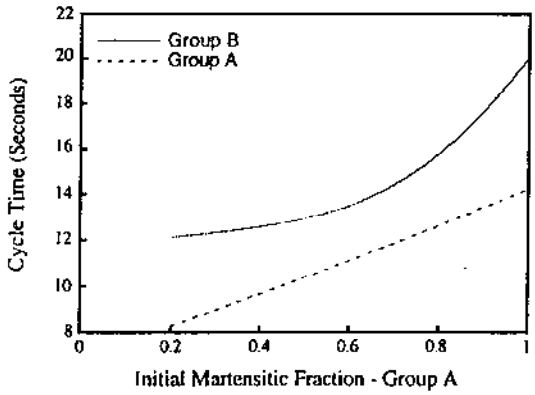

Figure 8. *Effect of an initial martensitic fraction of the group A and B wires on the cycle times.*

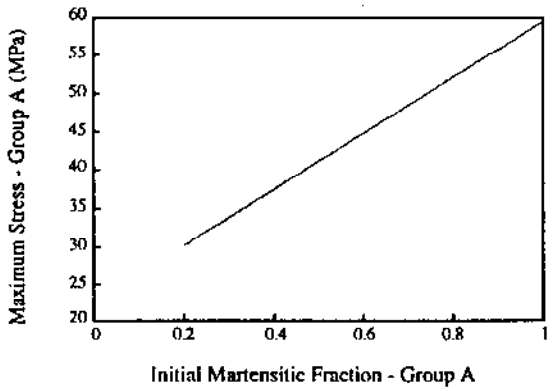

Figure 9. *Effect of the initial martensitic fraction of the group A wires on the maximum wire stress.*

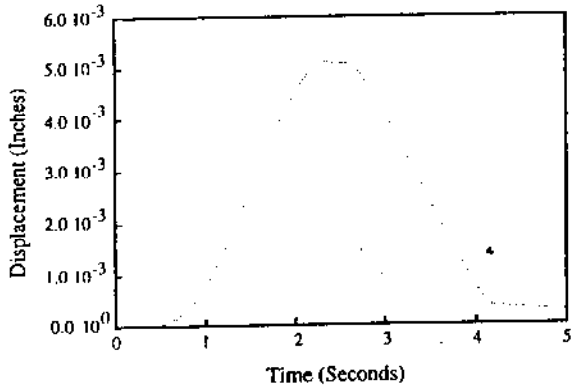

Figure 11. *Simulated differential actuator response with T_{max} = 100°C.*

higher stress. The maximum wire stress in the group A wires increases linearly with the initial martensitic fraction as shown in Figure 9. Increasing the initial martensitic fraction of the group A wires from 0.2 to 1.0 causes the wire stress to double. The increased stress increases the transformation temperatures resulting in longer cycle times.

The initial martensitic fraction of the group A wires also has an effect on the actuator stroke. Though increasing the martensitic fraction of the group A wires decreases the reset gap, it has the reverse influence on the stroke. Figure 10 shows the effect of the initial martensitic fraction of the group A wires on the actuator stroke. Increasing the martensitic fraction results in almost a 40% decrease in the actuator stroke. As a result, the martensitic fraction of the group A wires should be limited to the value that preserves reset.

Simulated Sinusoidal Response

The simulated response of the differential actuator and its associated control signals are shown in Figures 11 and 12, respectively. The physical parameters used for the simulation are the same as those in Table 1 except that $\xi_0^A = 0.9\xi_0^B$ and d = 0.005 inches. The frequency of oscillation depends on the maximum attainable wire temperature. For the maximum temperature given in Table 1, the response is nearly sinusoidal with a frequency of 0.3 Hz. As the maximum temperature is increased, the frequency of the response will increase as shown in Figure 13. Using a diameter of 5 millinches and a maximum temperature of 200°C above the austenite finish temperature, the maximum frequency of oscillation is 0.8 Hz (Figure 13). This is an improvement of 167% over previous designs (Baz et al., 1990b; Liang and Rogers, 1992) with similar material properties.

Since cooling is not used for either part of the actuation cycle, the maximum frequency is no longer limited by natural convection. Providing that small diameter wires are used in the subgroups, and that sufficient amplification is available to provide the input power, the differential force actuator is capable of operating in the range from 10 to 20 Hz. Table 2 gives the maximum wire temperatures required to maintain a 10 and 20 Hz bandwidth for a wire diameter of 5 millinches and indicates that relatively low maximum wire temperatures are required. As a result, differential force actuators are feasible for use as extended bandwidth actuators.

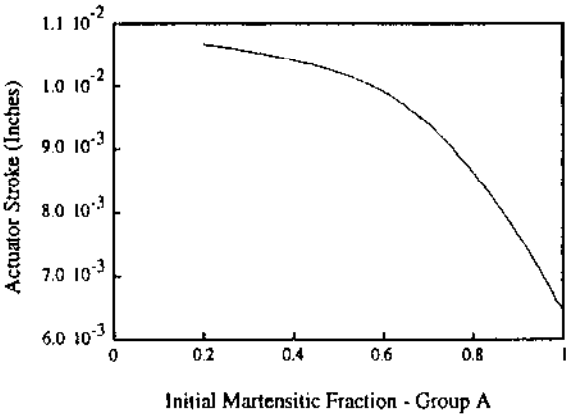

Figure 10. *Effect of the initial martensitic fraction of the group A wires on the actuator stroke.*

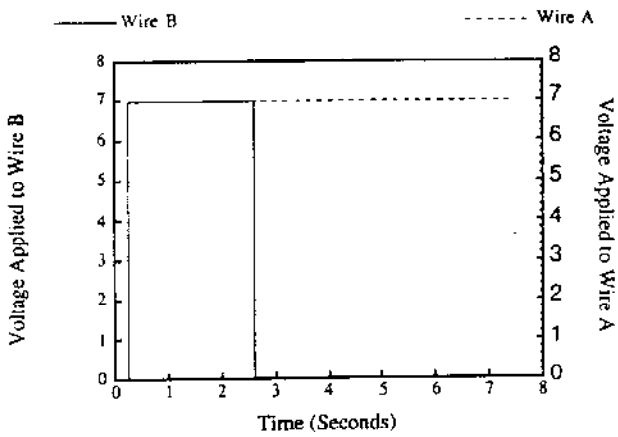

Figure 12. *Control signal for simulated differential actuator.*

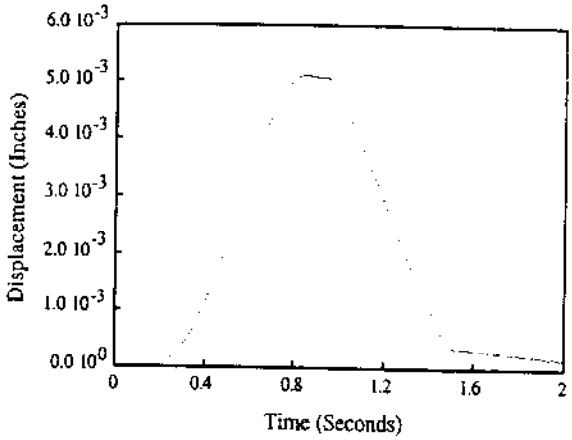

Figure 13. Simulated differential actuator response with T_{max} = 200°C.

EXPERIMENTAL RESPONSE OF THE DIFFERENTIAL ACTUATOR

Setup and Procedure

A photograph of the apparatus used for the differential force actuator tests is shown in Figure 14. The actuator consists of a single pair of wires, each two inches in length. The top and bottom sections of the actuator are affixed to the stand while the middle section is free to displace. The actuator displacement is monitored with an LVDT that is connected to the middle section. Set screws are used to attach the wires to the sections. A set of leads for resistive heating are connected to each wire, and thermocouples are used to monitor wire temperature. The thermocouples provide temperature feedback that allow the heating processes to be coordinated. An automated data acquisition system equipped with a digital signal processor is utilized to record temperature and displacement as well as to provide control signals.

Table 3 lists the physical parameters of the wires used for the tests. Two types of wires were employed. For the initial martensitic fraction tests, wires with a diameter of 25.0 millinches and an austenite start temperature of 27°C were used. For the actuator frequency tests, wires with a diameter of 7.5 millinches and an austenite start temperature of 27°C were utilized as well. In preparation for the tests, the wires were heated in an oven to a temperature of 100°C and then placed in a liquid nitrogen bath. This process set all of the wires to pure martensite, which was the reference state.

The group B wires were given initial martensitic strains by straining them while in the martensitic phase. For all of the tests, a martensitic strain of 8% was used. Straining while in this phase causes twin boundary movement which is later recovered by heating. The initial martensitic fractions in the A wire were obtained by heating it part, or all, of the way through the austenitic transformation. This process drives away part of the martensite that formed while in the liquid nitrogen bath. The temperature to which the A wire was heated depended on the desired initial martensitic fraction and will be discussed in the next section. Once both groups were set to their initial martensitic fractions, the wires were loaded into the fixture. Care was taken not to deform the wires during the loading process as this would change the initial martensitic fraction.

Table 2. Maximum wire temperatures required to maintain extended bandwidths.

Frequency Bandwidth	10 Hertz	20 Hertz
T_{max}	300°C	500°C

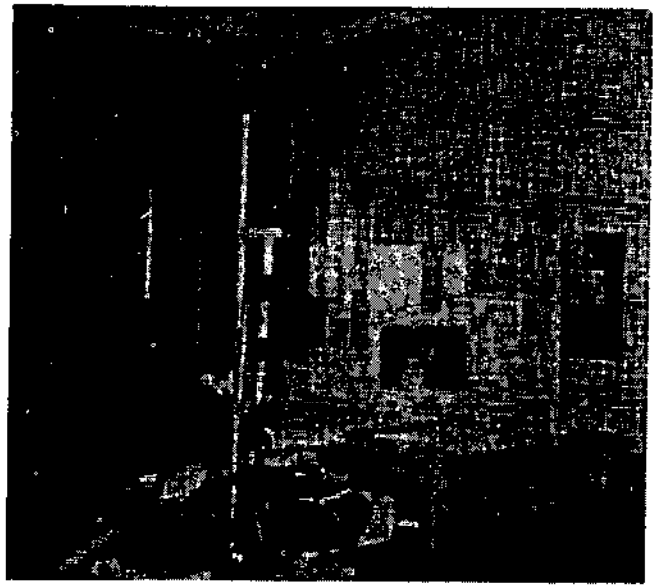

Figure 14. Differential actuator testing apparatus.

RESULTS

Initial Martensitic Fraction Ratio

Figures 15, 16, and 17 show the results of the initial martensitic fraction studies. Figure 15 gives the response of an actuator in which no stress induced martensite is formed in the A wire. The A wire for this test was heated completely through the austenitic transformation which left it with no initial martensite. In this case, the B wire recovered its initial strain but could not get the wire past its first yield point. No stress induced martensite formed, and as a result, the A wire had no strain martensitic structure to recover and could not return the actuator to its initial position. The small amount of recovery shown in Figure 15 is due to normal thermal contraction of wire B as it cools.

The A wire for the actuator whose response is shown in Figure 16 also had no initial martensitic fraction. In this

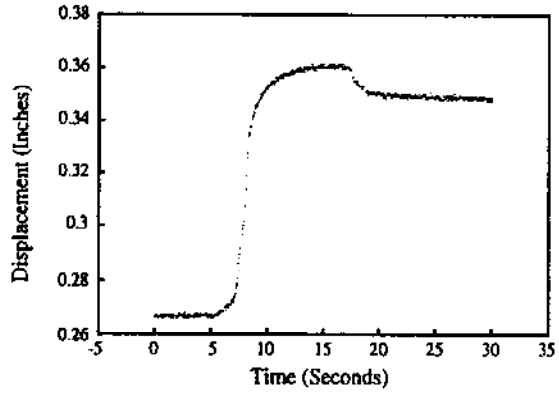

Figure 15. *Actuator cycle with no stress induced martensite in wire A which results in no strain martensitic to recover.*

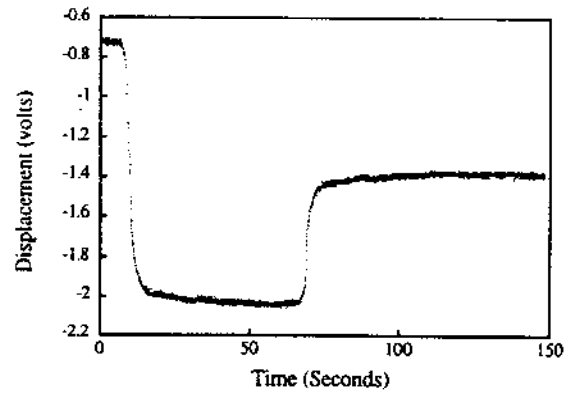

Figure 16. *Actuator cycle with no initial martensitic fraction in A wire, $\xi_0^A = 0$.*

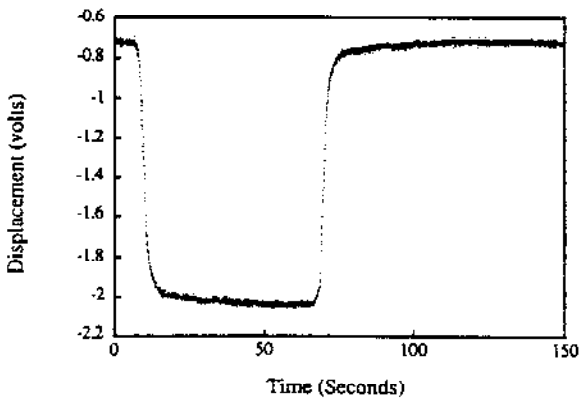

Figure 17. *Complete differential actuator cycle with $\xi_0^A = 0.9$ and $\xi_0^B = 0.72$.*

test, though, the stress generated by the B wire forced the A wire past the first yield point. As a result, some martensite was induced, but not enough to allow the A wire to return the actuator to its initial position. The force generated by the B wire only induced enough martensite to restore half of the original deformation.

Figure 17 shows a complete actuation cycle. In this test, the A wire was given an initial martensitic fraction equal to 0.9 times the initial martensitic fraction in wire B. The initial martensitic fraction of the B wire was 0.8. Therefore, the initial martensitic fraction of the A wire required to achieve complete recovery was 0.72. The temperature that the A wire needed to be heated to in order to reach a martensitic fraction of 0.72 was found to be 28°C. Preparing the A wire in this manner allows it to be able to fully recover the deformation caused by the B wire.

The results shown in Figures 15 through 17 support the existence of a critical martensitic fraction ratio. The numerical simulations indicate that the critical ratio of the martensitic fraction of the A wire to the martensitic fraction of the B wire is 0.9. The results shown in Figure 17 verify this value.

Maximum Actuator Frequency

Figures 18 and 19 show single actuation cycles for actuators containing two different wire diameters. A 3 amp current was used to heat the wires. The wire diameter affects the maximum attainable wire temperature and the thermal time constant, both of which reduce the actuation time. Figure 18 shows a cycle for an actuator with physical parameters equal to those in Table 3, a wire diameter of 25 millinches, and an initial martensitic fraction in the A wire of 0.72. Measurements of the time required to complete the cycle indicate that the actuator operates at a frequency of 0.1 Hz. The maximum frequency predicted by numerical simulation is 0.212 Hz. Figure 19 shows the response of the same actuator but with 7.5 millinch diameter wires. The oscillation frequency for this case is 1.667 Hz, while the frequency predicted in the numerical simulation is 1.853 Hz. In both

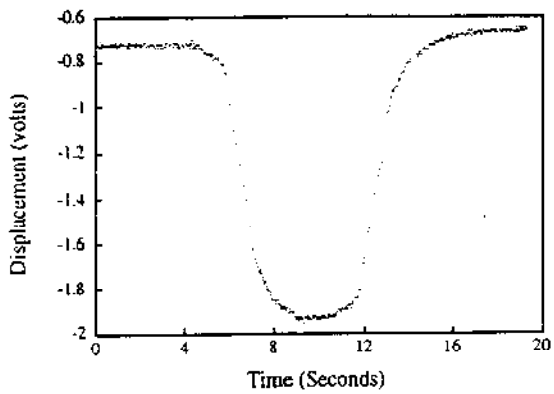

Figure 18. *Actuation cycle with d = 25.0 millinches: 0.1 Hz—Exp., 0.212 Hz—Num.*

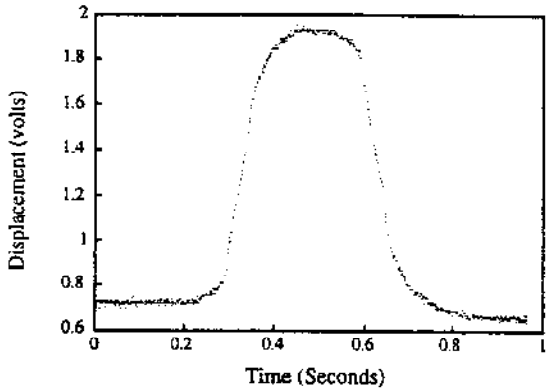

Figure 19. Actuation cycle with d = 7.5 millinches: 1.667 Hz—Exp, 1.853 Hz—Num.

cases, the experimental value is lower than the predicted value. The discrepancy is likely due to the non-ideal conditions under which the experiments were performed, which included excessive handling of the wires during setup, slippage in the gripping system during operation, and fluctuating ambient temperatures.

The results shown in Figure 18 and 19 indicate that the actuation frequency is very sensitive to the wire diameter. Simulations indicate that further reductions in the wire to 5 millinches would allow the actuator to achieve a 5–10 Hertz bandwidth. In order to optimize the actuation frequency, small diameter wires and high driving power should be used.

CONCLUSIONS

The purpose of this study was to investigate a method of extending the usable bandwidth of shape memory alloy actuators for vibration control. The differential actuator, which uses SMA wires in agonist-antagonist pairs, appears to be a solution despite the fact that it does not rely on cooling for the return cycle. Simulation shows that only modest power requirements are necessary to achieve bandwidths between 10 and 20 Hz. The results from the simulations and experiments also indicate that the ratio of the initial martensitic fraction of the group A wires to the group B wires must be greater than 0.9 in order to achieve a complete actuation cycle. If the ratio is less than this value, the group A wires will not be able to return the actuator in the initial position.

Table 3. Parameters for the experimental differential actuator.

Parameter	Value
M_s	0°C
M_f	−24.3°C
A_s	25.7°C
A_f	34.4°C
D	7000 MPa
L	2 in
θ	0.1 MPa/°C
Ω	−70 MPa
T_f	170,500°C
T_0^A	25°C
T_0^B	25°C
d	0.025, 0.0075 in
ξ_0^A	0, 0.72
τ_0^B	0.8
$n = N$	1
W	0.5 lb

NOMENCLATURE

A_s, A_f = austenite start and finish temperatures
D = elastic modulus
h = heat convection coefficient
L_A, L_B = length of the SMA wires in the different force actuator
M_s, M_f = martensite start and finish temperatures
s = wire cross-sectional area
T = temperature
T_f = final stable temperature of an SMA actuator
ϵ = engineering strain
ϵ_L = maximum amount of recoverable strain
ϵ_{res} = residual martensitic strain
θ = thermoelastic tensor
ξ^A, ξ^B = martensitic fraction in wire groups A and B, respectively
σ = stress
τ = thermal time constant
Ω = transformation tensor

Superscripts

A = variables related to wire group A of the differential actuator
B = variables related to wire group B of the differential actuator

Subscript

0 = denotes initial condition

REFERENCES

Baz, A., K. Imam and J. McCoy. 1990a. "Active Vibration Control of Flexible Beams Using Shape Memory Actuators", *Journal of Sound and Vibration*, 140(30):437–456.

Baz, A., K. Imam and J. McCoy. 1990b. "The Dynamics of Helical Shape Memory Actuators", *Journal of Intelligent Material Systems and Structures*, 1:105–133.

Baz, A. and J. Ro. 1992. "Thermo-Dynamic Characteristics of Nitinol-Reinforced Composite Beams", *Composites Engineering*, 2:(5–7):527–542.

Buehler, W. J. and C. R. Wiley. 1965. "Nickel Based Alloys", U.S. Patent 3,147,851, Naval Ordinance Laboratory.

Chaudhry, Z. and C. A. Rogers. 1991a. "Bending and Shape Control of Beams Using SMA Actuators", *Journal of Intelligent Material Systems and Structures*, 2:581–602.

Chaudhry, Z. and C. A. Rogers. 1991a. "Bending and Shape Control of Beams Using SMA Actuators", *Journal of Intelligent Material Systems and Structures*, 2:581–602.

Chaudhry, Z. and C. A. Rogers. 1991b. "Response of Composite Beams to an Internal Actuator Force", *Proceedings of the 32nd Structures, Structural Dynamics and Materials Conference*, AIAA-91-1166-CP, pp. 186–193.

Cross, W. B., A. H. Kariotis and F. J. Stimler. 1970. "Nitinol Characterization Study", No. GER-14188 (NASA-CR-1433), Goodyear Aerospace Corporation, Akron, Ohio.

Holman, J. P. 1981. *Heat Transfer*, McGraw-Hill Book Company, New York, pp. 240–250.

Jackson, C. M., A. H. Wagner and R. J. Wasilweski. 1972. "55-Nitinol—The Alloy with a Memory: It's Physical Metallurgy, Properties and Applications", NASA-SP-5110, Battelle Memorial Institute.

Liang, C. and C. A. Rogers. 1990. "One-Dimensional Thermomechanical Constitutive Relations for Shape Memory Materials", *Journal of Intelligent Material Systems and Structures*, 1:207–234.

Liang, C. and C. A. Rogers. 1991. "The Multi-Dimensional Constitutive Relations of Shape Memory Alloys", *Proceedings of the 32nd Structures, Structural Dynamics and Materials Conference*, AIAA-91-1165-CP, pp. 178–185.

Liang, C. and C. A. Rogers. 1992. "Design of Shape Memory Alloy Actuators", *Journal of Mechanical Design*, 114:223–230.

Materials Electronic Products Corp. 1990. *Thermoelectric Heat Pumps*, Materials Electronic Products Corp., New Jersey.

Quattrone, R. A. 1992. *Two-Way Force Actuators*, U.S. Patent Application 07/984619.

Rogers, C. A. and H. H. Robertshaw. 1988. "Development of a Novel Smart Material", *ASME 1988 Winter Annual Meeting*, 88-wa/DE-9, Chicago, IL, November 27–December 2.

Rogers, C. A., C. Liang and J. Jia. 1989a. "Behavior of Shape Memory Alloy Reinforced Composite Plates Part I. Model Formulations and Control Concepts", *Proceedings of the 30th Structures, Structural Dynamics and Materials Conference*, AIAA-89-1389-CP, pp. 2011–2017.

Rogers, C. A., C. Liang and J. Jia. 1989b. "Behavior of Shape Memory Alloy Reinforced Composite Plates Part II: Results," *Proceedings of the 30th Structures, Structural Dynamics and Materials Conference*, AIAA-89-1331-CP, pp. 1504–1513.

Rogers, C. A. and D. K. Barker. 1990a. "Experimental Studies of Active Strain Energy Tuning of Adaptive Composites", *Proceedings of the 31st Structures, Structural Dynamics and Materials Conference*, AIAA-91-1086-CP, pp. 2234–2241.

Rogers, C. A., C. R. Fuller and C. Liang. 1990b. "Active Control of Sound Radiation from Panels Using Embedded Shape Memory Alloy Fibers", *Journal of Sound and Vibration*, 136(1):164–170.

Rogers, C. A., C. Liang and J. Jia. 1991. "Structural Modification of Simply Supported Laminated Plates Using Embedded Shape Memory Alloy Fibers", *Computers and Structures*, 38(5/6):569–580.

Rogers, C. A. and C. Liang. 1993. "Design of Shape Memory Alloy Springs with Applications in Vibration Control", *Journal of Vibration and Acoustics*, 115:129–135.

Tanaka, K., T. Hayashi, Y. Itoh and H. Tobushi. 1992. "Analysis of Thermomechanical Behavior of Shape Memory Alloys", *Mechanics of Materials*, 13:207–215.

Wayman, C. M. and T. W. Duerig. 1990. "An Introduction to Martensite and Shape Memory Alloys", *Engineering Aspects of Shape Memory Alloys*, Butterworth-Heinemann, Boston, pp. 3–20.

Wilson, D. G., J. R. Anderson, R. D. Rempt and R. Ikegami. 1990. "Shape Memory Alloys and Fiber Optics for Flexible Structure Control", *Proceeding of the SPIE: Fiber Optic Smart Structures and Skins III*, 1370, pp. 286–295.